# The electronic states of 1,2,3-triazole studied by vacuum ultraviolet photoabsorption and ultraviolet photoelectron spectroscopy, and a comparison with ab initio configuration interaction methods

# The electronic states of 1,2,3-triazole studied by vacuum ultraviolet photoabsorption and ultraviolet photoelectron spectroscopy, and a comparison with ab initio configuration interaction methods

Michael H. Palmer, Søren Vrønning Hoffmann, Nykola C. Jones, Ashley R. Head, and Dennis L. Lichtenberger

Citation: The Journal of Chemical Physics **134**, 084309 (2011); doi: 10.1063/1.3549812
View online: http://dx.doi.org/10.1063/1.3549812
View Table of Contents: http://scitation.aip.org/content/aip/journal/jcp/134/8?ver=pdfcov
Published by the AIP Publishing

# The electronic states of 1,2,3-triazole studied by vacuum ultraviolet photoabsorption and ultraviolet photoelectron spectroscopy, and a comparison with *ab initio* configuration interaction methods

Michael H. Palmer,[1,a)] Søren Vrønning Hoffmann,[2,b)] Nykola C. Jones,[2,c)] Ashley R. Head,[3] and Dennis L. Lichtenberger[3,d)]
[1]*School of Chemistry, University of Edinburgh, West Mains Road, Edinburgh EH9 3JJ, Scotland, United Kingdom*
[2]*Institute for Storage Ring facilities (ISA), Aarhus University, Ny Munkegade 120, Building 1520, DK-8000, Aarhus C, Denmark*
[3]*Department of Chemistry and Biochemistry, The University of Arizona, Tucson, AZ 85721, USA*

(Received 19 August 2010; accepted 11 January 2011; published online 24 February 2011)

The Rydberg states in the vacuum ultraviolet photoabsorption spectrum of 1,2,3-triazole have been measured and analyzed with the aid of comparison to the UV valence photoelectron ionizations and the results of *ab initio* configuration interaction (CI) calculations. Calculated electronic ionization and excitation energies for singlet, triplet valence, and Rydberg states were obtained using multireference multiroot CI procedures with an aug-cc-pVTZ [5*s*3*p*3*d*1*f*] basis set and a set of Rydberg [4*s*3*p*3*d*3*f*] functions. Adiabatic excitation energies obtained for several electronic states using coupled-cluster (singles, doubles, and triples) and complete active space self-consistent field procedures agree well with experimental values. Variations in bond lengths with the electronic state are discussed. The lowest energy UV band (~5.5–6.5 eV) is assigned to three electronically excited states and demonstrates the occurrence of a nonplanar upper state on the low energy side. A UV photoelectron spectrum with an improved resolution yielded adiabatic and vertical ionization energies and reorganization energies for several of the lowest cationic states. As well as excitations to the *s*, *p*, *d*-Rydberg states are the excitations consistent with an *f*-series. © *2011 American Institute of Physics*. [doi:10.1063/1.3549812]

## I. INTRODUCTION

Electronic excitations and Rydberg states of molecules are fundamental to many molecular properties[1–4] and have attracted the attention of experimentalists[5,6] and theoreticians.[7–9] The molecule studied here is 1,2,3-triazole (**123T** in Fig. 1). Two complementary techniques are used to probe the excited electronic states. Vacuum ultraviolet (VUV) photoabsorption spectroscopy measures the electronic excitations of the neutral molecule, and UV photoelectron spectroscopy measures the positive ion states of the molecule in relation to the neutral ground state. Taken together, these two techniques assist in the identification of a Rydberg series for the neutral molecule, which converges to the ionization energy in the VUV photoabsorption spectrum. To help assign both spectra, several computational methods were used, including a method with the ability to calculate both the energies and electron distributions of *f*-orbitals and states. These calculations allow for the assignment of the Rydberg states in the VUV photoabsorption spectrum of **123T** as an uncommon *f*-series. The theoretical and experimental studies of **123T** lead to a detailed understanding of the changes in the electronic structure and the changes in the geometry that accompany them.

## II. EXPERIMENTAL AND COMPUTATIONAL DETAILS

### A. UV and VUV spectroscopy

The photoabsorption spectrum of **123T** was taken using the UV1 beamline on the ASTRID storage ring at Aarhus

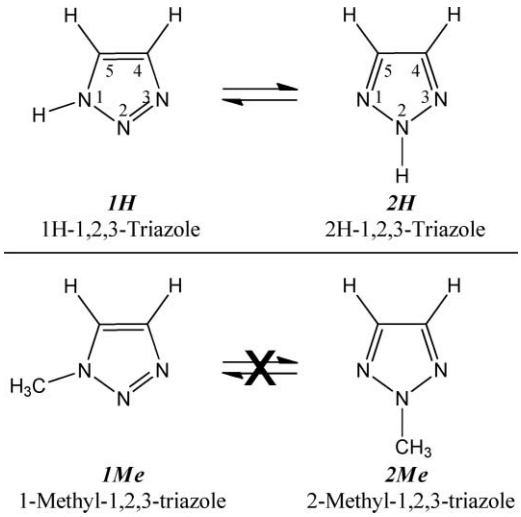


FIG. 1. The tautomeric structures **1H** and **2H** for 1,2,3-triazole (**123T**) and the tautomer-blocked methyl-1,2,3-triazole derivatives **1Me** and **2Me**. The numbering scheme of the triazole ring is shown for **1H** and **2H**.

a)Electronic mail: m.h.palmer@ed.ac.uk, Phone: +44 (0) 131 650 4765, Fax: +44 (0) 131 650 4743.
b)Electronic mail: vronning@phys.au.dk.
c)Electronic mail: nykj@phys.au.dk.
d)Electronic mail: dlichten@email.arizona.edu.

 

University, Denmark. The UV1 beamline and the experimental apparatus have been described in detail by Eden *et al.*[10] A toroidal grating monochromator provides a tuneable source of light with a resolution of 0.075 nm. The sample container and the gas cell (path length, $l = 15.5$ cm) were heated to maintain a constant temperature during measurements. The pressure of the gas in the cell was measured using a heated capacitance manometer and the pressure was chosen so that the attenuation of the light is kept low, thereby ensuring that saturation effects are negligible. The transmitted light ($I_t$) was measured using a photomultiplier tube (model 9402B, Electron Tubes, UK). The intensity of the incident light ($I_0$) was recorded with the cell evacuated. Absolute photoabsorption cross-sections ($\sigma$) are then obtained using the Beer–Lambert law. **123T** for this and all experiments was purchased from Sigma-Aldrich. The VUV spectrum of **123T** initially showed characteristic water photoabsorptions as expected because **123T** is hygroscopic. After freeze–pump–thaw cycles to remove air and continued vacuum pumping on the sample, this impurity disappeared. The final spectrum was taken with the sample at 35 °C, with a spectral range from 245 nm (5.058 eV) to 115 nm (10.772 eV) in 0.1 nm intervals.

### B. Gas-phase photoelectron spectroscopy

He I and He II spectra were recorded on an instrument built around a 360 mm mean radius, 80 mm gap hemispherical analyzer (McPherson) with photon sources, calibration, data collection, and analysis techniques that have been described previously.[11–13] The sample was loaded into a Young's tube under an inert atmosphere to minimize exposure to water. The sample was vaporized at room temperature with a water impurity as evidenced by a small peak at 12.62 eV that was subtracted from the spectra. More details of the data collection and analysis are provided in the supplementary material,[14] including instrument calibration, resolution, and corrections.

### C. Theoretical methodology and computational details

*Ab initio* calculations were performed with the GAMESS-UK[15] and MOLPRO[16,17] suites of programs. All excited state and ionic equilibrium structures were optimized using a cc-pVTZ basis set consisting of C,N(11*s*,6*p*,1*d*)/H(5*s*,1*p*) contracted to [5*s*,3*p*,1*d*]/[3*s*,1*p*]. To check for consistency, these states were studied by coupled-cluster (singles, doubles, and triples) [CCSD(T)], complete active space self-consistent field (CASSCF), and B3LYP methods. The CASSCF number of active MO's for $a_1$, $b_1$, $b_2$, and $a_2$ symmetries were 2, 4, 2, and 3, respectively, allowing several equilibrium structures to be obtained. Increasing the active space to include further $\sigma^*$ and $\pi^*$ MOs showed very little difference in the structures obtained.

For the vertical CI study, the basis set used was aug-cc-pVTZ C,N(10*s*5*p*3*d*1*f*) contracted to [5*s*3*p*3*d*1*f*], with H [3*s*3*p*2*d*]. These were augmented with a [4*s*3*p*3*d*3*f*] set of Rydberg functions with *s,p,d,f* exponents as in our previous work.[18] The vertical ionization energies were determined by Greens' function (GF) and Tamm–Dancoff approximation (TDA) calculations.[15] Zero-point vibrational energies and thermal contributions to free energies in the gas phase were calculated by the B3LYP/cc-pVTZ model.

Our multireference multiroot configuration interaction module (MRD-CI) code[19–21] is now able to process *f*-orbitals and *f*-electronic states[18,22] and was used for the main CI study. All 22 valence electrons, together with the lowest 165 virtual orbitals were active. The MRD-CI calculations used up to ~180 spin combinations of two and four open-shell main reference configurations, which are expanded with up to eight open shells at the CI stage by single and double excitations. All CI calculations were performed at the corresponding $\tilde{X}^1A_1$ ground state equilibrium geometry. The molecule lies in the *y, z* planes with the Rydberg set at the center of mass. In the discussion of Rydberg states, we denote $p_x$, $d_{xz}$, $f_{xxx}$ etc. states, as *X*, *XZ*, *XXX*, etc. For simplicity, *XX* is used instead of $X^2$. Most virtual molecular orbitals are relatively pure Rydberg types; however, the *Z*-MO's do mix with *XX*–*YY* at the SCF level. The $C_{2v}$ components (and numbers of combinations within each symmetry representation) of the *d*-Rydberg set are ($X^2$–$Y^2$) and (3*ZZ*–*RR*) ($2a_1$ symmetry), *XY* ($1a_2$), *XZ*($1b_1$), and *YZ*($1b_2$); the *f*-set are: (*ZZ*–*XX*–*YY*)*Z* and (*XX*–*YY*)*Z*, ($2a_1$); (*YY*–*ZZ*)*X* and (*XX*–*YY*–*ZZ*)*X* ($2b_1$); (*XX*–*ZZ*)*Y* and (*YY*--*XX*–*ZZ*)*Y* ($2b_2$), *XYZ* ($1a_2$).

## III. RESULTS

### A. Structural issues

Discussion of the structure of **123T** begins with consideration of the tautomers 1H-1,2,3-triazole (**1H**) and 2H-1,2,3-triazole (**2H**) shown in Fig. 1. An early ultraviolet photoelectron spectroscopy (UPS) study[23] adopted the structure of the **1H** form, which at that time was the only tautomer known. Both the **1H** and **2H** tautomers were later identified in the gas phase by microwave spectroscopy[24,25] and the **2H** tautomer by electron diffraction.[25] The ratio of **2H**:**1H** was determined to be approximately 1000:1.[24,25] This predominance of the **2H** form was supported by the UPS comparison[26,27] of the tautomeric mixture with the "blocked" pair of *N*-methyl compounds (Fig. 1, compounds **1Me** and **2Me**). The energies of the tautomers calculated by CCSD(T) and B3LYP methods indicate a predominance of the **2H** tautomer in the gas phase with a **2H**:**1H** population ratio at an equilibrium of 1500:1 according to the electronic energy, 700:1 with the zero-point vibrational energy correction, and 300:1 according to the free energy at 298.15 K (B3LYP values). These experimental and calculated ratios combined with the UPS study of **1Me** and **2Me** indicate that the **1H** tautomer should make a negligible contribution to the UPS spectra and the VUV photoabsorption spectra.

The equilibrium structures obtained by the CCSD(T) method for the neutral **2H** and the first four ionic states of **2H** are shown in Fig. 2; B3LYP density functional theory calculated equilibrium structures for these states, which are similar to the CCSD(T), are given in the supplementary material.[14] Coupling of the cation and excited electronic states can distort structures away from $C_{2v}$

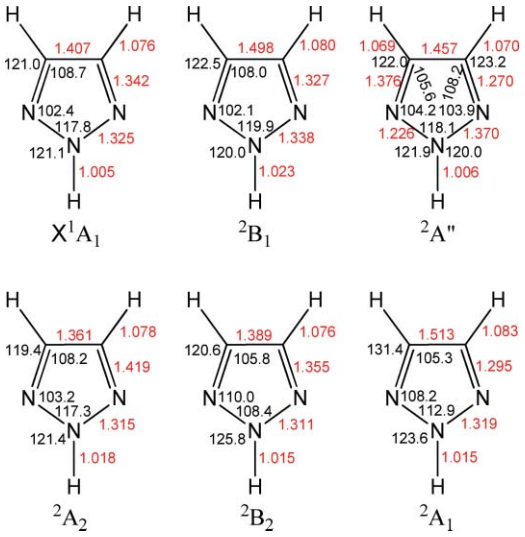


FIG. 2. Bond angles and bond distances of the 2H-1,2,3-triazole neutral ground state ($X^1A_1$), the ground cation state in $C_{2v}$ ($^2B_1$) and $C_s$ ($^2A''$) symmetry, and higher ionic states in $C_{2v}$ symmetry calculated using the UCCSD(T)/cc-pVTZ methodology.

symmetry; this possibility was explored for the first cation and lowest singlet and triplet excited states of **2H**. With the UCCSD(T), CASSCF, and UB3LYP methods, where the leadıng "U" refers to unrestricted open shell methods, the electronic energy of the lowest cation state minimizes to a planar ($C_s$) structure in which one N–N bond is lengthened and the other is shortened, with concomitant changes in other bond distances and angles (Fig. 2). This is a symmetric double minimum potential surface with distortion in either direction from the $C_{2v}$ saddle point. However, the electronic energy is stabilized only 47 $cm^{-1}$ from the $C_{2v}$ saddle point, while the

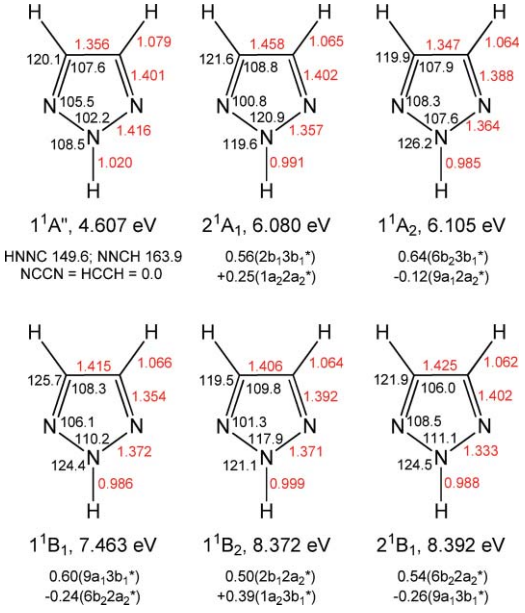


FIG. 3. Structures and relative energies of the lowest singlet electronically excited state in $C_s$ symmetry ($1^1A''$) and selected higher singlet states in $C_{2v}$ symmetry of 2H-1,2,3-triazole, calculated using a CASSCF/pVTZ [14e,11MO] methodology. The energies are referenced to the ground state energy of –240.92831 a.u.

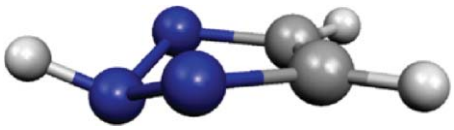

FIG. 4. The global minimum structure of the lowest triplet excited state of 2H-1,2,3-triazole ($3A''$, $C_s$ symmetry) contains a pyramidal nitrogen atom in the two position.

smallest vibrational frequency in the molecule is 551 $cm^{-1}$ (B3LYP), so the distortion energy is a minor perturbation of the energy of the lowest state.

The lowest singlet state ($^1A_2$) is optically forbidden; however, evidence will be presented that the UV photoabsorption onset shows evidence of doubling of lines, as observed in molecules where the excited state is nonplanar.[28–30] Hence we have studied the $C_s$ symmetry species which might exhibit this phenomenon, and these clearly show that minor distortions into $C_s$ symmetry can lead to the optically forbidden state becoming allowed. The optimized structure of the lowest singlet state to the nonplanar $C_s$ symmetry is shown in Fig. 3. Also, the lowest vibrational frequency corresponds to a wag of the N–H bond in and out of the plane of the molecule. Some excited states show nonplanar $C_s$ symmetry in which the energy minimizes with this N–H group out of the plane of the molecule, and the planar structure is then a saddle point between two equivalent minima. An example for the lowest triplet state is shown in Fig. 4. Most of the following discussion will be with reference to the $C_{2v}$ structures and energies, which has the advantage of separate labels for the electronic states.

### B. UV photoelectron spectrum

The ground-state electronic configuration of **2H** in $C_{2v}$ symmetry contains doubly occupied MO's up to: $9a_1^2$, $6b_2^2$, $1a_2^2$, and $2b_1^2$.[27] These orbitals, illustrated in Fig. 5, are the origins of the low energy ionizations and electronic excitations. The full He II photoelectron spectrum (Fig. 6) shows the same features as the previous spectra,[23,26] but close examination of individual ionization bands at the higher

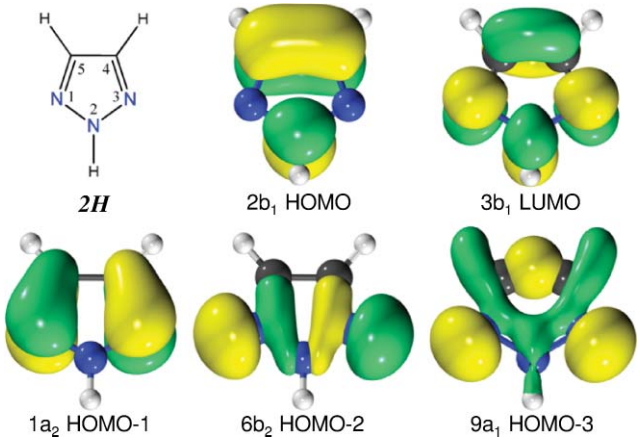


FIG. 5. The orbital isosurfaces (value = ±0.05) for the valence and lowest unoccupied orbitals of 2H-1,2,3-triazole. These orbitals were calculated using B3LYP/cc-pVTZ method.

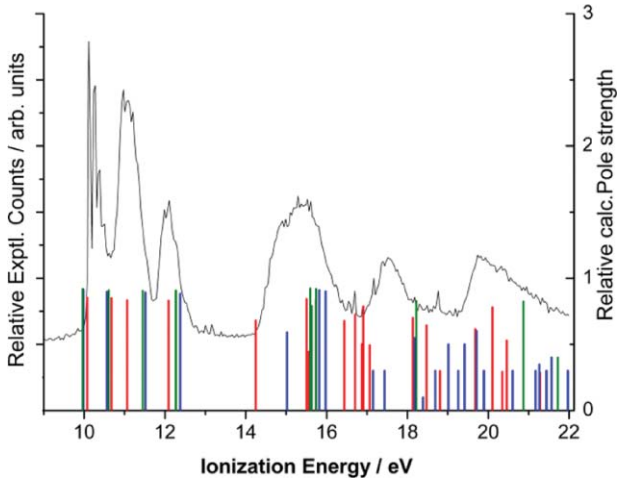


FIG. 6. The He II photoelectron spectrum of 2H-1,2,3-triazole with superimposed theoretical ionic states calculated from MRI-CI in red, TDA in blue, and GF in green [see the supplementary material (Ref. 17) for calculated values].

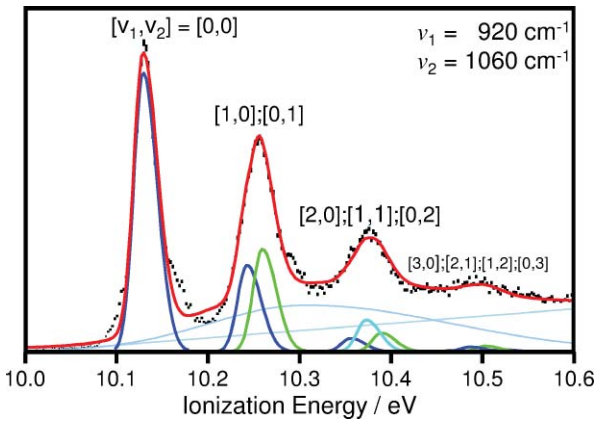


FIG. 7. Vibrational analysis of the first ionization band in the He I photoelectron spectrum of 2H-1,2,3-triazole. The black dots are the experimental data and the red line is the sum of the two vibrational progressions modeled as Poisson distributions (the light blue lines account for electron scatter in the spectrometer).

resolution of this spectrometer reveals complex vibrational structure in several of the bands. The vibrational progression in the first ionization band is shown in Fig. 7. The width of the first peak is the instrumental linewidth at this kinetic energy, so the position of this peak is the adiabatic ionization energy [10.128(2) eV]. The instrument broadening and the electron scattering around the base of the peak are minor contributions to the standard deviation of the peak position obtained from three experiments. The calculations reproduce the first adiabatic ionization energy well (Table I). For comparison to the **2H** tautomer, the first adiabatic ionization energy of the **1H** tautomer was also calculated by the UB3LYP method, yielding a value of 9.75 eV and reorganization energy of 0.3 eV. The spectra show no evidence of ionization intensity from 9.5 to 10 eV, confirming that ionizations from the **1H** tautomer do not make a visible contribution to the photoelectron spectrum.

The successive broadening of the peaks at higher vibrational quanta from 10.2 to 10.6 eV in the first band indicates the presence of at least two vibrational modes of different frequencies. A two-mode Poisson model similar to methods published previously[31–33] produces the vibrational quanta and the vibrational progression shown in Fig. 7. All individual vibrational peaks are constrained to the same width, so after the position, width, and intensity of the [0,0] peak are determined, the only parameters in the analysis are the vibrational frequency and the Huang-Rhys factor $S$ for each vibrational mode, where $S$ is the single parameter that determines the relative intensity of all vibrational components in the Poisson distribution. These values then provide the reorganization energy [0.083(3) eV] and the effective vertical ionization energy [10.211(5) eV].

The primary distortion of the molecule that occurs with ionization to the $^2B_1$ positive ion state is the symmetric lengthening of the C–C distance (Fig. 2). The UB3LYP calculation of the normal vibration modes of this cation shows two $A_1$ vibrational modes that correspond to this distortion, with frequencies of 967 and 1127 $cm^{-1}$. Using a typical scaling factor of 95% to compare calculated vibrational frequencies with experimental vibrational frequencies yields values of 909 and 1071 $cm^{-1}$, which agree within uncertainty to the

TABLE I. The experimental adiabatic ionization energies of 2H-1,2,3-triazole from the UV photoelectron data compared with the calculated values from two different computational methods (all energies in eV).

| | | Calcd. adiabatic IE | | Calcd. Vertical IE | Reorganization energy[b] |
|---|---|---|---|---|---|
| Expt. adiabatic IE[a] | Symmetry | CCSD(T)[c] | UB3LYP[d] | CCSD(T) | CCSD(T) |
| 10.128 ± 0.002 | $^2B_1$ | 10.039 | 10.127[e] | 10.194 | 0.155 (0.083 ± 0.003) |
| 10.70 ± 0.05 | $^2A_2$ | 10.53 | 10.55 | 10.80 | 0.28 (0.25 ± 0.1) |
| 10.85 ± 0.05 | $^2B_2$ | 10.61 | 10.56 | 11.17 | 0.55 (0.25 ± 0.1) |
| 11.80 ± 0.05 | $^2A_1$ | 11.70 | 11.54 | 12.06 | 0.36 |

[a]The first adiabatic IE is the position of the first vibrational component. The uncertainty of the first ionization is the standard deviation of three measurements. The adiabatic IEs of the other states are estimates from ionization onsets due to unresolved vibrational components.
[b]$IE_V$–$IE_A$, the experimental value is in parentheses.
[c]CCSD(T) ground state energy –241.8367211 a.u.
[d]B3LYP ground state energy –242.3193604 a.u.
[e]Including zero-point energy correction (ZPE), 10.130 without ZPE.

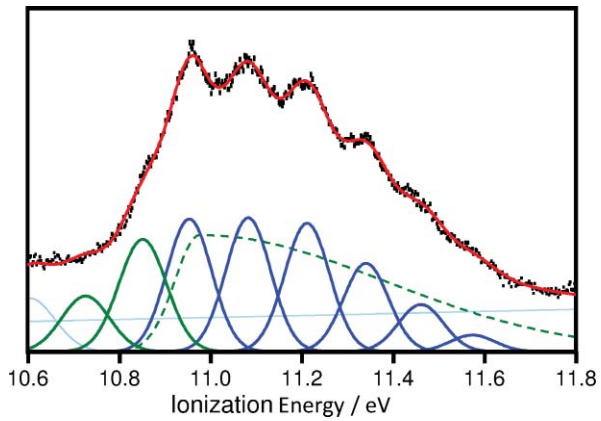


FIG. 8. Vibrational analysis of the second ionization band in the He I photoelectron spectrum of 2H-1,2,3-triazole. The black dots are the experimental data and the red line is the sum of the vibrational progressions modeled as Poisson distributions. The blue peaks represent a vibrational mode of one cation state and the green peaks are a second state with the dashed green line modeling unresolved intensity. The light blue line is intensity from instrument scattering.

experimental values of 920(20) and 1060(20) $cm^{-1}$ from the analysis of this ionization.

As illustrated in Fig. 8, the improved resolution of the second ionization band, from about 10.7 to 11.8 eV, shows a complex band profile that suggests vibronic coupling with contributions from two cation electronic states. The calculations indicate that the two states in this band are the $^2A_2$ and the $^2B_2$. The energies of these two states are close and cannot be clearly differentiated by this experiment, but the calculations consistently predict the $^2A_2$ to be slightly below the $^2B_2$ in energy. The more resolved vibrational progression (the blue peaks in Fig. 8) is modeled with a Poisson intensity distribution of vibrational peaks with a frequency spacing of 1040(40) $cm^{-1}$. The Huang-Rhys factor $S = 1.7$ is taken from the intensity ratios of peaks $v = 1$ through 4. The other electronic state is evidenced by shoulders on the leading edge of the ionization (the green peaks in Fig. 8) and unresolved intensity to the high energy side of the band, indicated by the dashed line. The Huang-Rhys factor ($S = 1.9$) is taken from the ratio of the first two peaks with vibrational quanta $v = 0$ and $v = 1$.

The third ionization band in Fig. 6, from about 11.8 to 12.5 eV, shows a complex intensity profile and detailed analysis is not attempted (see close-up of this band in the supplementary material[14]). The low-IE portion of the band shows broad, unresolved vibrational intensity reminiscent of the vibronic coupling and broadening in the second ionization band of pyrrole.[34–36] The complexity of the band profile prevents a clear determination of adiabatic and vertical ionization energies. The onset of ionization intensity is listed in Table I as the approximate adiabatic ionization energy, and the point in this region with the greatest intensity is listed as the vertical ionization energy in Table II. The remaining bands in the spectrum (ionization energies greater than 14 eV) are calculated to contain multiple ionizations (supplementary material[14]) and specific assignments are not attempted.

The three computational methods used to calculate the vertical ionization energies in Table II give similar results and agree well with experimental values. The numerical fit is best for the MRD-CI set illustrated in red in Fig. 6. The vertical values show very little difference between TDA and GF for the low-IE range. The calculated adiabatic ionization energies ($IE_A$) and reorganization energies in Table I are also similar for both methods and also reproduce the experimental values. Franck–Condon calculation of the vibrational profile was not attempted due to the complexity of the coupling in the vibrational wave functions discussed earlier in Sec. III. The calculated sequence of the cation states as shown by $IE_A$ is: $2b_1^{-1}$ $(\pi) < 1a_2^{-1}$ $(\pi) \leq 6b_2^{-1}$ $(\sigma, LP_N^-) < 9a_1^{-1}$ $(\sigma, LP_N^+)$. This calculated sequence is in agreement with previous work.[26,27] The calculated character of these orbitals is shown in Table III, where considerably different characters of the $6b_2$ and $9a_1$ orbitals are apparent.

### C. VUV photoabsorption spectrum

#### 1. Valence states

Figure 9 shows the VUV photoabsorption spectrum with superimposed vertical valence states. The energy sequence up to 6 eV of the calculated vertical valence states (Table IV) using the *s-, p-, d-, f*-basis set is $^1A_2 < {}^1A_1 \sim {}^1B_1$, with excitations from each of the three highest occupied MO's. These are assigned to the broad UV band lying between 5.4 and 6.6 eV. This band shows a broad structure with a series of weak maxima on both the leading and trailing edges (Fig. 10). The spacing of this structure is most easily seen in Fig. 10(b), which shows the deviation of the absorption intensity from that of a single broad asymmetric Gaussian approximating the entire band. The overall energy origin of

TABLE II. Selected vertical ionization energies from the UV photoelectron data and calculations of 2H-1,2,3-triazole with different methods (all energies in eV).

| | | | MRD-CI [b] | | TDA | GF |
|---|---|---|---|---|---|---|
| Expt. vertical IE[a] | Symmetry | Open + vacant shell occupancy | Calcd. IE | $c_i^2$ | Calcd. IE | Calcd. IE |
| 10.21 ± 0.005 | $^2B_1$ | $2b_1$ | 10.08 | 0.85 | 9.98 | 9.97 |
| 10.95 ± 0.1 | $^2A_2$ | $1a_2$ | 10.68 | 0.85 | 10.56 | 10.61 |
| 11.10 ± 0.1 | $^2B_2$ | $6b_2$ | 11.07 | 0.83 | 11.52 | 11.45 |
| 12.12[c] ± 0.02 | $^2A_1$ | $9a_1$ | 12.09 | 0.83 | 12.38 | 12.27 |

[a]The ionizations listed as a range are ionization bands that include multiple unresolved ionizations.
[b]Ground state energy $\tilde{X}^1A_1$ –241.45685839 a.u.
[c]The value given is the position in the band with the greatest intensity.

TABLE III. SCF level Mulliken analyses (of electrons) of occupied MO's which relate to the Rydberg study.

| | | $N_2$ | | $N_1$ and $N_3$ | | $C_4$ and $C_5$ | | $H_4$ and $H_5$ | |
|---|---|---|---|---|---|---|---|---|---|
| Symmetry | lone pair Type | *s* | *p* | *s* | *p* | *s* | *p* | *s* | *p* |
| $6b_2$ | $LP_N^-$ | 0.000 | 0.044 | 0.090 | 0.371 | 0.012 | 0.021 | 0.001 | 0.000 |
| $9a_1$ | $LP_N^+ + CC$ | 0.008 | 0.001 | 0.082 | 0.211 | –0.001 | 0.164 | 0.023 | 0.001 |
| | $\pi$-orbitals | *p* | *d* | *p* | *d* | *p* | *d* | *p* | *d* |
| $1a_2$ | $\pi_3$ | 0.000 | 0.015 | 0.382 | 0.0 | 0.092 | 0.017 | 0.002 | 0.001 |
| $2b_1$ | $\pi_2$ | 0.315 | 0.001 | 0.007 | 0.011 | 0.308 | 0.005 | 0.005 | 0.002 |

the band is 5.578 eV (44 992 $cm^{-1}$). The lowest energy transition is shown in greater detail in the inset in Fig. 10. The doubling of the first transition is seen by the two main peaks of equal intensity in this region. The red peaks model the doubling and the fine structure. In this simulation, all peak widths are constrained to be the same, and the intensities of corresponding peaks in the doublet are also constrained to be equal, so there are few variable parameters in the fit. Even with these constraints, the symmetric doublet model gives a good representation of the observed intensity profile. The separation of the two main peaks in the doublet is 0.0318(5) eV (256 $cm^{-1}$). The corresponding separation in 1,2,5-oxadiazole, which shows the same phenomenon, is 191 $cm^{-1}$.[29,37,38]

Although this fine structure is not clearly observed in the higher-energy transitions, the transitions up to ~6.2 eV are represented very well [Fig. 10(a)] by symmetric double peaks based on a two-peak representation as in the first transition, but with the smaller fine structure in the doublet unresolved due to the overlap between peaks. Figure 10(b) assists observation of the spacings between the doublets and shows that in some cases the finer structure is evident. The doubled transitions are shown with different colors in the figure to clarify the symmetric pairs. There is a suggestion of two vibrational frequencies, one nearly twice the other, so that they nearly coincide in every other transition and give rise to this intensity pattern. The average and standard deviation of the energy spacing between the centers of consecutive doublets is 0.069(4) eV or 553(32) $cm^{-1}$, which matches the calculated lowest vibrational frequency in the molecule of 551 $cm^{-1}$ mentioned previously.

From around 6.2 eV to higher energy, the contours of the band [again shown more clearly in Fig. 10(b)] settle into a series with a spacing of 0.043 ± 0.003 eV (340 ± 25 $cm^{-1}$). Attempts to model this region with a doubling of the transitions were not successful, but the behavior is typical of anharmonicity high in a potential well.

After this broad peak from 5.4 to 6.6 eV there is a gap in the spectrum followed by rising structure at 6.8 to 7.3 eV. The calculated valence excitation energies contain a gap of ~1 eV, so valence states do not account for the structure in this region. The discussion below shows that the lowest Rydberg state occurs here. The group of valence states calculated between 7.3 and 8.5 eV is assigned to the broad and complex structure observed between 7.5 and 9 eV, but with

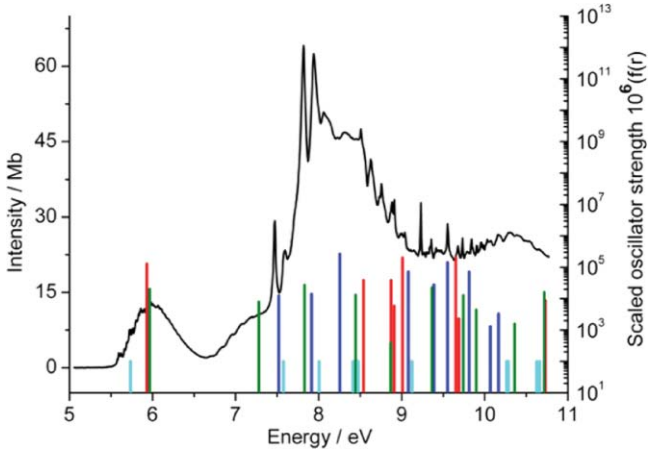


FIG. 9. The VUV photoabsorption spectrum for 2H-1,2,3-triazole with the calculated valence state energies superimposed and color-coded by symmetry. $^1A_1$ (red), $^1B_2$ (blue), $^1B_1$ (olive), $^1A_2$ [cyan, shown with arbitrary $f(r)$ set to $10^{-4}$].

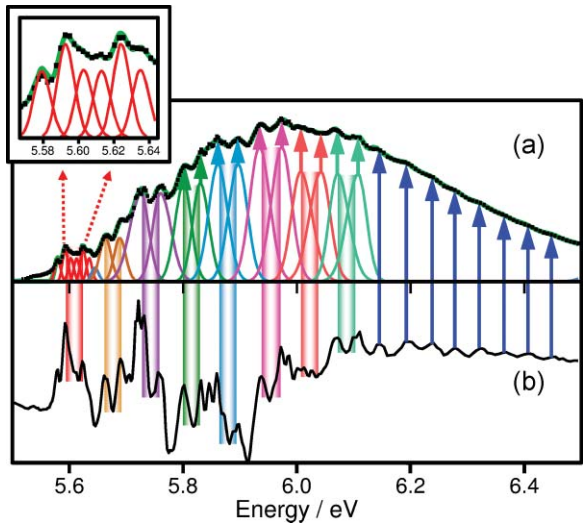


FIG. 10. Examination of the structure in the first band of the VUV photoabsorption spectrum of 2H-1,2,3-triazole. The black dots in **(a)** are the experimental data and the line shown in **(b)** visibly accentuates the structure by showing the deviation of the absorption intensity from that of a single broad asymmetric Gaussian (halfwidth = 0.55 eV) approximating the entire band. In **(a)** the green line is the fit of the data modeled with constrained symmetric doublets (color-coded) up to 6.1 eV, based on the structure at 5.6 eV (red peaks, inset). The vertical arrows from **(b)** to **(a)** show the alignment of the structure revealed in **(b)** with the doublets in **(a)** up to 6.1 eV and the progression beyond 6.1 eV.

TABLE IV. Selected calculated singlet valence states for 2H-1,2,3-triazole: vertical excitation energies, oscillator strengths, and second moments (a.u.).[a,b,c,d]

| Energy (eV) | $10^6$ $f(r)$ | Symmetry | State ($c_i^2 > 0.02e$, in decreasing density) | $\langle x^2 \rangle$ | $\langle y^2 \rangle$ | $\langle z^2 \rangle$ |
|---|---|---|---|---|---|---|
| 0.0 | | $A_1$ | $\tilde{X}^1A_1$ $9a_1 6b_2 2b_1 1a_2$ | −23.2 | −25.2 | −15.7 |
| 5.74 | 0 | $A_2$ | $6b_2 3b_1$* | −26.0 | −23.6 | −17.0 |
| 5.93 | 129 240 | $A_1$ | $2b_1 3,4b_1$* | −27.2 | −26.2 | −17.6 |
| 5.97 | 19 904 | $B_1$ | $9a_1 4b_1$* + $1a_2 7b_2$* | −30.5 | −40.0 | −21.1 |
| 7.28 | 7877 | $B_1$ | $2b_1 10a_1$* | −36.2 | −35.5 | −41.4 |
| 7.52 | 12 426 | $B_2$ | $1a_2 4b_1$*+ $2b_1 2a_2$* | −27.4 | −28.3 | −23.5 |
| 7.58 | 0 | $A_2$ | $1a_2 10,11a_1$* | −35.5 | −31.1 | −47.3 |
| 7.83 | 26990 | $B_1$ | $2b_1 11a_1$* | −33.7 | −34.6 | −60.2 |
| 7.92 | 14163 | $B_2$ | $6b_2 11a_1$* | −35.6 | −31.0 | −60.4 |
| 8.01 | 0 | $A_2$ | $1a_2 12a_1$* + $2b_1 9b_2$* | −36.1 | −43.5 | −36.5 |
| 8.26 | 263 913 | $B_2$ | $1a_2 4b_1$* − $2b_1 2_2$* | −35.4 | −32.1 | −22.0 |
| 8.41 | 0 | $A_2$ | $2b_1 7b_2$* | −32.8 | −62.3 | −40.6 |
| 8.45 | 12 965 | $B_1$ | $2b_1 12a_1$* | −35.0 | −42.8 | −38.4 |
| 8.48 | 0 | $A_2$ | $1a_2 11,10a_1$* | −38.5 | −41.4 | −61.9 |
| 8.54 | 38 334 | $A_1$ | $2b_1 4,3b_1$* | −40.6 | −29.2 | −20.7 |
| 8.87 | 385 | $B_1$ | $1a_2 7b_2$* − $9a_1 4b_1$* | −32.9 | −51.4 | −25.2 |
| 8.87 | 38 616 | $A_1$ | $9a_1 10,11a_1$* $1a_2 3a_2$* | −35.6 | −32.7 | −51.8 |
| 8.91 | 5828 | $A_1$ | $9a_1 11a_1$* $6b_2 7b_2$* $1a_2 3a_2$* | −37.4 | −47.7 | −52.0 |
| 9.01 | 201 174 | $A_1$ | $1a_2 3,4,2a_2$* | −36.4 | −35.1 | −21.5 |
| 9.08 | 71 624 | $B_2$ | $6b_2 10,11a_1$* | −42.2 | −41.2 | −48.3 |
| 9.13 | 0 | $A_2$ | $2b_1 8b_2$* + $1a_2 12a_1$* | −35.4 | −48.1 | −41.1 |
| 9.36 | 22 456 | $B_1$ | $2b_1 13,15a_1$* | −35.2 | −52.0 | −31.6 |
| 9.39 | 27 975 | $B_2$ | $6b_2 12a_1$* | −34.2 | −37.8 | −48.7 |
| 9.55 | 142 568 | $B_2$ | $2b_1 3,2,4a_2$* | −38.7 | −39.0 | −20.0 |
| 9.65 | 202 337 | $A_1$ | $1a_2 2a_2$* + $2b_1 4b_1$* | −42.0 | −29.0 | −29.6 |
| 9.69 | 2288 | $A_1$ | $2b_1 5b_1$* | −36.4 | −35.1 | −21.5 |
| 9.74 | 12 864 | $B_1$ | $1a_2 8,9b_2$* | −31.9 | −49.7 | −42.9 |
| 9.81 | 71 086 | $B_2$ | $1a_2 5,3b_1$*+ $1b_1 2a_2$* | −37.4 | −27.1 | −25.9 |
| 9.90 | 4438 | $B_1$ | $2b_1 14a_1$* | −43.2 | −39.2 | −61.6 |
| 10.07 | 1296 | $B_2$ | $1a_2 3,5b_1$* | −49.1 | −28.9 | −30.5 |
| 10.17 | 3307 | $B_2$ | $9a_1 7b_2$* | −39.4 | −69.9 | −50.2 |
| 10.26 | 0 | $A_2$ | $2b_1 8b_2$* − $1a_2 14a_1$* | −36.9 | −53.9 | −54.1 |
| 10.28 | 0 | $A_2$ | $1a_2 14a_1$* − $2b_1 7b_2$* | −37.7 | −50.4 | −57.8 |
| 10.36 | 1596 | $B_1$ | $2b_1 15a_1$* | −40.0 | −47.0 | −65.6 |
| 10.63 | 0 | $A_2$ | $2b_1 10b_2$* | −37.6 | −70.2 | −49.7 |
| 10.66 | 0 | $A_2$ | $1a_2 12a_1$* | −32.1 | −44.2 | −48.8 |
| 10.72 | 15 938 | $B_1$ | $1a_2 9b_2$* | −36.6 | −72.8 | −73.7 |
| 11.45 | 1981 | $A_1$ | $2b_1 6b_1$* | −37.6 | −36.8 | −21.6 |
| 11.47 | 520 | $B_2$ | $2b_1 3,4a_2$* | −40.9 | −42.8 | −26.2 |

[a]Basis sets (C,N/H [7*s*4*p*3*d*/4*s*2*p*2*d*]).
[b]B3LYP (−242.32319 a.u.) orbital occupancy $1a_1^2 - 9a_1^2 1b_2^2 - 6b_2^2\ 1b_1^2\ 2b_1^2 1a_2^2$.
[c]Excitation energies are relative to the $\tilde{X}^1A_1$ ground state CI energy −241.59009 a.u.
[d]Singly occupied orbitals except where shown; active MO's 6–110.

no discernable detail to allow specific comparisons. The VUV photoabsorption spectrum does not drop to the baseline in the 9–11 eV region; again a number of valence states are calculated for that region. A full table with all the calculated valence states is provided in the supplementary material,[14] and these states are consistent with the overall spectrum.

### 2. Rydberg states

Rydberg states formed by excitation to a particular upper state will follow the sequence,

$$\text{Term value} = \text{IE} - E = \frac{R}{(n-\delta)^2}, \quad (1)$$

where $R$ is the Rydberg constant (13.606 eV), $n$ is the principal quantum number (PQN), and $\delta$ is the quantum defect (QD).[39–41] The principal Rydberg states identified are shown in Table V. Selected calculated Rydberg states are listed in Table VI, and a full listing of all the states is provided in the supplementary material.[14] All the lowest calculated Rydberg states arise from $2b_1$ ($\pi_3$) excitation and are shown in Fig. 11 overlaid on the VUV photoabsorption spectrum. The spacing and the intensity pattern of several of the Rydberg transitions correlate well with the vibrational progression observed in the first ionization in the UPS spectrum, as illustrated in Fig. 12. The rising absorption above ~6.68 eV has a similar vibrational spacing. However, the intensity of the vibrational bands on $IE_1$ decreases in its vibrational progression on the

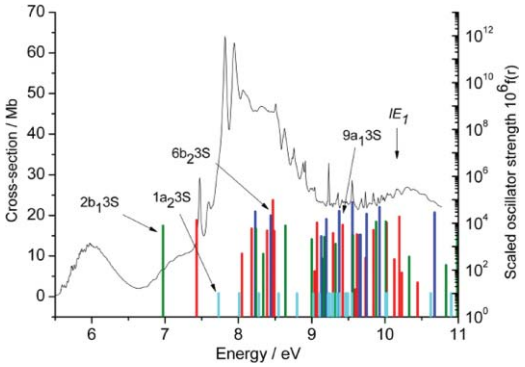


FIG. 11. The VUV photoabsorption spectrum for 2H-1,2,3-triazole with the calculated aug-cc-pVTZ + SPDF basis Rydberg state energies superimposed and color-coded by symmetry. $^1A_1$ (red), $^1B_2$ (blue), $^1B_1$ (olive), $^1A_2$ [cyan, shown with arbitrary f(r) set to $10^{-5}$].

high energy side, whereas the VUV photoabsorption starting from ~6.68 eV has an increasing trend with indications of an underlying valence state. The absorption band starting from 6.68 eV is assigned to the $2b_1 3s$ state with an energy from the electronic structure calculations of 6.96 eV. The high energy side of the band overlaps with a calculated valence state at 7.52 eV ($\pi\pi^*$ $1a_2 4b_1^* + 2b_1 2a_2^*$).

The next two observed Rydberg state origins at 7.471 and 7.814 eV are explained by $2b_1 3p$ states. The quantum defects (0.74 and 0.58) are quite high. The calculated $3p$ states are predicted to lie in the order $X < Y < Z$, with $X$ (7.43 eV) and $Z$ (8.24 eV) having nonzero oscillator strengths. The band at 7.471 eV is assigned to $2b_1 3X$. The difference in the calculated energy for the $2b_1 3Z$ state is rather larger than desired, but the assignment of pure $Z$-MO's is difficult owing to mixing with $XX$–$YY$ at the SCF level.

Further, $IE_1$ vibrational sequences[14] have origins at 8.510 and 9.231 eV. These can be correlated with a group of higher bands to be $2b_1 nd$ or $2b_1 nf$ sequences and are the most prominent in the spectrum. Individual measurements show $\delta$ ~0.1; it is attractive to assign the whole group from 8.510 to 9.958 eV as an $nd$-series which fits Eq. (1) with $IE_1$ = 10.123(2) eV and $\delta$ 0.097(4), where $IE_1$ is very close to the experimental value 10.128(2) eV (Table I). At this point, the results indicate a $2b_1 nd$ series. This type of series is not unknown, with similar long sequences being found for pyrrole ($1a_2 nd$)[42,43] and furan ($1a_2 nd$);[44] both of these molecules are isoelectronic with **123T**. However, if the 8.510 eV band is included in a plot of energy versus $(1/n^*)$ where $n^* = n - \delta$, then the extrapolated value for $IE_1$ rises to 10.137(2) eV. If the 8.510 eV band is omitted, $IE_1$ is 10.133(2) eV with correlation coefficient –0.99998, and the discrepancy with the observed $IE_1$ is reduced. The 8.510 eV band sits on an intensity plateau, with an overall intensity of 47 Mb. The higher set of six bands shows a slightly declining 30–25 Mb variation without this plateau. Thus the 8.510 eV band seems too weak, relative to the underlying continuum, to fit with the higher members. Furthermore we calculate the $d$-states to be very weak; the most intense of the calculated $3d$ components of the $2b_1 nd$-series are $2b_1 3XY$, $2b_1 3XZ$, and $2b_1 3(3ZZ–RR)$. Thus we conclude that the higher group of bands, 9.231 up to 9.958 eV, forms a separate $2b_1 nf$ series. Small differences between the first and higher member of an apparent series are critical to correct assignment. The quantum defect for the apparently $1a_2 3d$ state (7.525 eV) in furan was anomalous when compared to the higher $nd$ members.[44] Subsequently, a strong band at 8.01 eV in furan was observed in the (3 + 1) resonance-enhanced multiphoton ionization (REMPI) spectrum[45,46] where it was assigned as an $1a_2 4f$ state on the grounds that the $1a_2 3d$ analogue was not observed.

Several of the $f$-Rydberg states of **2H** lie above the level accessible to the present basis set, but the fit of eight calculated Rydberg energies (Fig. 13) yields a $\delta$ of 0.1030(104) and converges on $IE_1$ with an extrapolated energy of $E_0$ = 10.1240(21) eV (with standard deviation in parentheses). This result is extremely close to the value from the photoelectron spectrum [10.128(2) eV)]. The figure also shows a plot of the energy versus $1/n^2$, and a tight fit with a single line is obtained.

A cluster of states is calculated in the range 8.47–8.9 eV (Table VI). The state at 8.472 eV is especially intense with $f(r)$ = 0.096, and although classified as a $4f$-Rydberg state, $2b_1 3(YY–ZZ)X$ is in reality a valence state. This state is

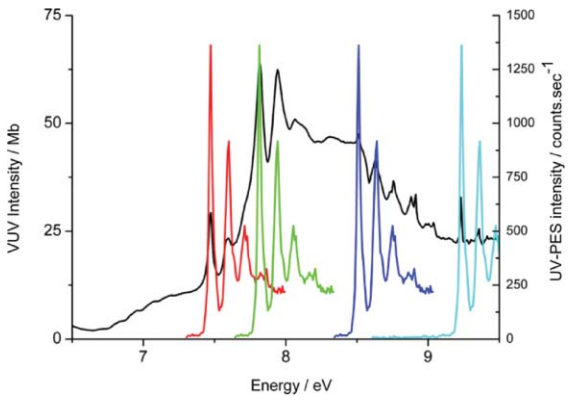


FIG. 12. The superposition of the lowest UPS ionization energy band profile on the VUV photoabsorption spectrum, indicating the presence of Rydberg states with term values 2.661 (red), 2.318 (green), 1.622 (blue), and 0.898 eV (cyan).

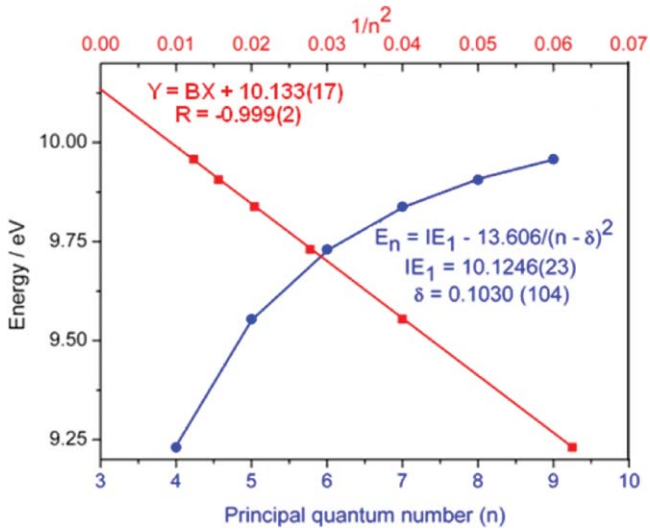


FIG. 13. The $f$-Rydberg series identified for 2H-1,2,3-triazole.

expected to be visible in the VUV spectrum and can possibly be assigned to the broad maximum at 8.6 eV in the VUV photoabsorption spectrum in Fig. 11.

The fine structure in the UPS envelope discussed above suggests that $IE_2$ ($^2A_2$) and the $IE_3$ ($^2B_2$) lie close to 10.70(5) and 10.85(5) eV, respectively. We assign the band origins at 7.946 eV (Table V) to excitation involving $^2B_2$ as the strongly allowed $6b_2 3s$ state, since the $1a_2 3s$ state is electronically forbidden. Conversely, we assign the band at 8.634 eV to the $1a_2 X$ state.

### 3. Lowest triplet state energies

The calculated sequence of the eight lowest triplet states (Table VII) is the same for both adiabatic and vertical excitation. The lowest adiabatic triplet states, both $\pi\pi^*$, are $^3B_2$ ($1a_2 3b_1^* + 2b_1 2a_2^*$) at 4.06 eV and $^3A_1$ ($2b_1 3b_1^* - 1a_2 2a_2^*$) at 4.98 eV, using the CASSCF excitation energies. The adiabatic excitation energies to the four triplet states having a similar upper state $3b_1^*$ leading term (representing excitations from the valence orbitals $2b_1$ at 4.98 eV, $1a_2$ at 4.06 eV, $6b_2$ at 5.47 eV, and $9a_1$ at 6.76 eV) do not match the sequence of IE for the valence MO's, so comparison with the sequence of ionization energies is difficult.

## D. Structural changes in the adiabatic singlet, triplet valence, and ionic state calculations

The calculations provide insight into the structural changes that occur with both ionization and electronic excitation. The ionic state structures optimized with CASSCF and B3LYP calculations[14] were found to agree well with the rigorous UCCSD(T) level results that are shown in Fig. 2. In the present discussion of the cation states, the UCCSD(T) results are used. There are three main bond length variables: NN (*a*), NC (*b*) and CC (*c*, all in Å). The HN and HC bonds vary by small amounts and are ignored. The change in bonds *a, b,* and *c* upon excitation ($X^1A_1$–state) is $\delta a$, $\delta b$, and $\delta c$. In the $^2B_1$ and $^2B_2$ cation states, $\delta a$, $\delta b$, and $\delta c$ are less than $\pm 0.03$ Å. In the $^2A_2$ cation state, a loss of $N_3C_4$ bonding character causes a larger $\delta c$ of 0.04 Å. For the $^2A_1$ cation state, the loss of $C_4C_5$ $2p\sigma$ bonding causes a $\delta c$ of –0.11 Å.

The equilibrium structures of several electronic excited states obtained by using CASSCF in $C_{2v}$ symmetry are shown in Fig. 3 and in the supplementary material.[14] The singlet and triplet states show $\delta a$, $\delta b$, and $\delta c$ differences for similar orbital occupancy. For the excited singlet states, almost all of the bonds increase in length on excitation ($\delta a$, $\delta b$, $\delta c$ are negative). An exception is $2^1A_2$, where $\delta b$ is +0.06 Å and is accompanied by a very large $\delta c$ −0.18 Å. This state is dominated by $9a_1 2a_2^*$ excitation and can be compared with the $^2A_1$ cation state where a large $\delta c$ also occurs. For the excited triplet states, most of the bond lengths increase, with the $\delta c$ for $1^3B_2$ and $1^3A_2$ as an exception. The largest change is –0.17Å for $\delta c$ in $2^3A_2$, which is the same as observed for the corresponding singlet in the same dominant configuration. The most variable bond upon excitation is the $C_4C_5$ bond. The 2H-1,2,3-triazole system can be thought of as an (NH) bridged buta-1,3-diene with diaza substitution (N replacing C), and this variability of the $C_4C_5$ bond is mirrored in the behavior of the central $C_2C_3$ bond in buta-1,3-diene.[18]

The bond length ratio (BLR) *b/c* gives a measure of the double/single bond character; for the $\tilde{X}^1A_1$ ground state, the *b/c* ratio is 0.943, and for the ionic states $^2B_1$ 0.943, $^2A_2$ 1.043, $^2B_2$ 0.975, and $^2A_1$ 0.856. With similar ratios to the ground state, the $^2B_1$ and $^2B_2$ ionizations occur with very little structural change. Major skeletal movement is required for the $^2A_2$ and $^2A_1$ states. The first pair can thus be expected to show dominant 0–0 bands in the photoelectron spectrum, whilst the latter pair will show a more Gaussian distribution of vibrational bands. In the excited state cases, the *b/c* ratio is close to the $\tilde{X}^1A_1$ ground state for $1^{1,3}A_1$ and $1^{1,3}B_1$ but is raised in $1^{1,3}A_2$ and $2^1A_1$. It is remarkably diminished in $2^{1,3}A_2$, which reflects the lengthening of the $C_4C_5$ bond more than the $N_3C_4$ change in the $9a_1 2a_2^*$ state. The triplet state BLR for $1^3B_2$, $2^3B_1$, and $1^3A_1$ are all increased, with few of the remaining states showing a reduction in BLR.

TABLE V. Observed Rydberg states and probable interpretations.[a]

| Energy (eV) | Intensity (MB) | Term value | Probable PQN (*n*) | QD ($\delta$) | Assigned IE | Rydberg state | Calcd. energy (eV) |
|---|---|---|---|---|---|---|---|
| 6.720 | 2.3 | 3.412 | 3 | 1.003 | $IE_1$ | $2b_1 3s$ | 6.965 |
| 7.471 | 29 | 2.661 | 3 | 0.739 | $IE_1$ | $2b_1 3p$ | 7.433 |
| 7.814 | 65 | 2.318 | 3 | 0.577 | $IE_1$ | $2b_1 3p$ | 8.237 |
| 8.510 | 47 | 1.622 | **3** | 0.104 | $IE_1$ | $2b_1 \mathbf{3}d_{ZZ-RR}$ | 8.392 |
| 9.231 | 33 | 0.898 | **4** | 0.103(10) | $IE_1$ | $2b_1 \mathbf{4}f$ | 8.472 |
| 9.554 | 29 | 0.578 | **5** | | | $2b_1 \mathbf{5}f$ | 9.294 |
| 9.730 | 26 | 0.400 | **6** | | | $2b_1 \mathbf{6}f$ | 10.023 |
| 9.838 | 25 | 0.294 | **7** | | | $2b_1 \mathbf{7}f$ | |
| 9.906 | 24 | 0.226 | **8** | | | $2b_1 \mathbf{8}f$ | |
| 9.958 | 25 | 0.174 | **9** | | | $2b_1 \mathbf{9}f$ | |
| 10.031 | 26 | 0.101 | | 0.393 | $IE_1$ | | |
| 7.946 | 62 | 2.904 | 3 | 0.835 | $IE_3$ | $6b_2 3s$ | 8.225 |
| 8.634 | 41 | 2.216 | 3 | 0.522 | $IE_2$ | $1_{a2} 3_{pX}$ | 8.440 |

[a]A fit of the data to $E(n) = E_0 - 13.606/(n-\delta)^2$ gave: $E_0 = 10.1246$ (23) (0.02%) $\delta = 0.1030$ (104) (10.1%) rms of residuals: $3.7 \times 10^{-3}$ variance of residuals (reduced $\chi^2$): $1.38 \times 10^{-5}$.

TABLE VI. Selected calculated singlet Rydberg states ex aug-cc-pVTZ [5*s*3*p*3*d*1*f*] + Rydberg [4*s*3*p*3*d*3*f*] (SPDF) basis set; vertical excitation energies (eV), oscillator strengths, and second moments (a.u).[a,b,c]

| Energy (eV) | $10^6$ f(r) | Symmetry | State | $\langle x^2\rangle$ | $\langle y^2\rangle$ | $\langle z^2\rangle$ |
|---|---|---|---|---|---|---|
| | | | $\tilde{X}^1A_1$ $9a_1 6b_2 2b_1 1a_2$ | −23.3 | −25.2 | −15.8 |
| 6.97 | 7794 | $B_1$ | $2b_1$S | −50.9 | −66.4 | −53.7 |
| 7.43 | 13 297 | $A_1$ | $2b_1X$ | −169.5 | −70.1 | −74.3 |
| 7.73 | 0 | $A_2$ | $1a_2$S | −52.8 | −63.8 | −57.3 |
| 8.01 | 0 | $A_2$ | $2b_1Y$ | −62.4 | −144.5 | −61.1 |
| 8.05 | 502 | $A_1$ | $2b_1XX$-$YY$ | −173.5 | −215.7 | −69.9 |
| 8.18 | 5854 | $A_1$ | $2b_1XZ$ | −199.7 | −81.2 | −179.7 |
| 8.23 | 31 193 | $B_2$ | $6b_2$S | −53.5 | −61.6 | −57.6 |
| 8.24 | 5691 | $B_1$ | $2b_1Z$ | −50.4 | −50.6 | −112.3 |
| 8.28 | 0 | $A_2$ | $2b_1YZ$ | −78.8 | −195.4 | −180.2 |
| 8.34 | 491 | $B_1$ | $2b_1$S | −297.6 | −283.8 | −309.9 |
| 8.39 | 4848 | $A_1$ | $2b_1ZZ$-$RR$ | −56.0 | −47.6 | −78.1 |
| 8.44 | 21 153 | $B_2$ | $1a_2X$ | −132.3 | −55.4 | −56.6 |
| 8.47[d] | 95 861 | $A_1$ | $2b_1(YY$-$ZZ)X$ | −72.7 | −48.5 | −44.2 |
| 8.49 | 4659 | $A_1$ | $2b_1(XX$-$YY$-$ZZ)X$ | −265.4 | −288.1 | −75.6 |
| 8.55 | 0 | $A_2$ | $1a_2Z$ | −46.2 | −43.8 | −101.2 |
| 8.64 | 7811 | $B_1$ | $1a_2Y$ | −60.4 | −135.4 | −60.1 |
| 8.80 | 0 | $A_2$ | $2b_1(XX$-$ZZ)Y$ | −55.6 | −115.0 | −103.1 |
| 9.00 | 2058 | $B_1$ | $2b_1(XX$-$YY)Z$ | −67.7 | −115.5 | −83.0 |
| 9.00 | 113 | $B_1$ | $1a_2YZ$ | −75.5 | −183.3 | −174.5 |
| 9.02 | 0 | $A_2$ | $1a_2$S | −303.9 | −289.2 | −321.8 |
| 9.04 | 89 | $A_1$ | $2b_1X$ | −124.7 | −54.5 | −79.3 |
| 9.07 | 10 436 | $A_1$ | $2b_1ZZ$-$RR$ | −89.8 | −63.9 | −128.4 |
| 9.11 | 0 | $A_2$ | $2b_1(XX$-$ZZ)Y$ | −92.2 | −214.6 | −232.0 |
| 9.13 | 2741 | $B_2$ | $2b_1XYZ$ | −203.0 | −203.5 | −191.7 |
| 9.16 | 322 | $B_1$ | $2b_1(ZZ$-$XX$-$YY)Z$ | −204.4 | −129.9 | −291.3 |
| 9.17 | 2594 | $B_1$ | $2b_1(XX$-$YY)Z$ | −142.7 | −211.1 | −170.0 |
| 9.20 | 14 970 | $B_2$ | $2b_1XY$ | −171.4 | −172.0 | −60.3 |
| 9.22 | 0 | $A_2$ | $2b_1(YY$-$XX$-$ZZ)Y$ | −238.2 | −255.0 | −66.5 |
| 9.24 | 0 | $A_2$ | $6b_2X$ | −122.6 | −49.4 | −53.1 |
| 9.29 | 3794 | $A_1$ | $2b_1(YY$-$ZZ)$X | −239.7 | −89.3 | −251.0 |

[a]B3LYP (−242.32319 a.u.) orbital occupancy $1a_1^2 - 9a_1^2 1b_2^2 - 6b_2^2\ 1b_1^2\ 2b_1^2 1a_2^2$.
[b]Excitation energies are relative to the $\tilde{X}^1A_1$ ground state CI energy −241.590088 a.u.
[c]Singly occupied orbitals except where shown.
[d]See text.

The angles in the four cations in Fig. 2 show that angle NNN is always larger than NNC or NCC. Most of the angles are close to those of the ground state, except for $^2A_1$, where a considerable lengthening of $C_4C_5$ is accompanied by the opening of the $N_3C_4H$ angle. This increase in bond length implies a move toward dissociation to 2 HCN molecules. In contrast, $^2B_1$ shows a lengthening of $C_4C_5$ accompanied by NNN opening and possibly tending toward dissociation to a NCCN molecule. The largest angle change for the singlet states is in $2^1A_2$, where a similar dissociation toward 2 HCN molecules appears to be happening. In this case the occupancy is $9a_1 2a_2$*.

Along with these changes in bond distances and angles, many of the excited states deviate from planarity. For example, the global minimum structure of the triplet excited states is calculated to be $^3A''$ ($C_s$ symmetry) with a pyramidal nitrogen atom as shown in Fig. 4. The corresponding singlet state has similar structure. This structure derives most directly from the $1a_2$ to $3b_1$ excitation with substantial reorganization energy.

## IV. DISCUSSION

The analysis given above for the 5.5–6.5 eV range of the VUV photoabsorption spectrum shows that a regularly spaced set of Poisson model bands was able to give a very tight fit (Fig. 10) to the full range of the observed spectrum. The 75.3 $cm^{-1}$ separation of the low energy (red) set of bands is much lower than any molecular frequency. Richardson reports an analogous doubling of 1,2,5-oxadiazole (isoelectronic with **2H**) and related molecules.[29,30,38] He attributed the doubling to the nonplanarity of the $\pi\pi^*$ state excited state in which the aromaticity of the molecule was partially destroyed.[29] The similar structure in the VUV photoabsorption spectrum of **2H** is explained with this argument, and a barrier to planarity is calculated to be ∼215 $cm^{-1}$.

The frequency interval of the rest of the present band is 553(32) $cm^{-1}$. The theoretical calculations (Table IV) suggest that three electronic states should be assigned to the observed envelope. These consist of both $\pi\pi^*$ ($^1A_1$) with a high oscillator strength, and $LP_N\pi^*$ ($^1B_1$ and $^1A_2$). The only common feature is that the LUMO ($3b_1$*) is prominent in all the

excitations. The observation of fairly regular vibrational states throughout the whole range of the band is surprising, since it seems improbable that three separate electronic states ($A_2$, $A_1$, and $B_1$) will all have nearly identical and aligned frequencies, suggesting coupling between the states into a complex system. Clearly, the present fit is only a pragmatic suggestion, but serves to help illustrate the nature of the vibrational structure in the band. The coupling between the states could occur, for example, by spin-orbit coupling or by vibrations and distortions that lower the symmetry. Such a phenomenon has been discussed in detail of the assignment of the Wulf band in the ozone UV spectrum.[47–49] Early assignments to the forbidden $^1A_2$ state were modified to include spin-orbit coupling of $^3A_2$, $^3B_1$, and $^1B_2$ states.[48,49] The $^1B_2$ state itself is responsible for the higher energy Hartley band in ozone.[47] We have shown that nonplanar forms of 1,2,3-triazole have significance in both the ions ($^2A''$), and the singlet and triplet manifolds (Figs. 2–4); mixing of states could well result in the deceptively simple analysis [Fig. 10(b)] appearing to work for the 5.5 to 6.5 eV band.

Assignment of the 3*s*, 3*p*, and 3*d* Rydberg states (Table V) is unambiguous; in contrast, we assign the sequence with energies from 9.23 to 9.96 eV, as an *f*-series rather than continuation of the 8.510 eV *d*-series, as discussed above. We have to note that there is a coincidence in the values for the quantum defect for the 3*d* and 4*f* series. However, the present value for $\delta$ of 0.0970(3) is close to our redetermination of the buta-1,3-diene *f*-series[18] where we found $\delta$ to be 0.0765(76). *f*-Rydberg states have not been commonly observed in polyatomic molecules, but the classic series in buta-1,3-diene[2,3,40] shows that there is no reason for them to be excluded from consideration.

We suspect that one reason for *f*-series not being more commonly recognized is that there are relatively few calculations where all of the spherical harmonics with *s, p, d, f* are treated equivalently. It is possible that some sequences for molecules related to the present study are 4*f*- rather than 4*d*-series, especially since the typical $\delta$ values are similar for both series. This possibility is currently under investigation. We have previously noted[44] that the quantum defect for an apparently 4*d* state in furan at 7.525 eV, which was based upon the $^2A_2$ ionic state, had an anomalous quantum defect when compared to the 3*d* analogue. This series had previously been labeled as $1a_2nf$ by Cooper *et al.*[46] The *f*-assignment was chosen because the $n = 3$ member was missing. This state has now been confirmed as one of the two *f*-Rydberg series in furan.[45,50] As in the furan study,[50] 2 + 1 REMPI spectroscopy has proved important in detecting *f*-Rydberg series, at least in part from the high resolution and use of several levels ($n + 1$) of multiphoton excitation. Seven Rydberg series, including 1*s*, 3*p*, 2*d*, and 1*f*, have been identified from the excitation of vinyl bromide.[51] Further examples can be expected, but *f*-Rydberg series are well established for polyatomic molecules. The VUV spectrum of cyclohexane ($C_6H_{12}$)[52] shows a prominent Rydberg series with members $n = 4$–9 converging on an $IE_1$ at 9.88 eV but has a missing $n = 3$ member. This absence was thought to be obscured by the continuum at 8.18 eV, but the perdeutero-molecule where the bands are displaced, does not show an $n = 3$ member either. Such examples warrant further examination for potential *f*-Rydberg states. Further historically interesting examples are given by Robin,[39–41] but these are generally limited to either diatomics or heavy-atom containing polyatomics.

Some of the calculated *f*-states have high oscillator strength in comparison with most Rydberg states. One possible reason for the intensity enhancement may be that the $\pi\pi^*$-valence states of mainly *p*-character mix with states with two levels of spherical harmonic higher, i.e., *p, f*-interactions. A similar interaction is often observed for *s, d*-interactions. In both of these situations, the lower valence states are dominated by the *s, p* components, but this mixing has a complementary effect on the *d, f* higher states. At the suggestion of a reviewer, we have considered two other possibilities: (a) that the *f*-Rydberg states observed here, have gained intensity ("giant resonances") through "orbital collapse". Such cases lead to valence rather than Rydberg states, as evidenced by the bands being present in the condensed phase as well as the vapour.[53] The only case where such a phenomenon could occur here is the 8.47 eV Rydberg band (Table VI); the high intensity is consistent with a valence state, although the state electron density is clearly as indicated a (*YY--ZZ)X* (i.e., *f*-type) state. A further interesting alternative (b) has been

TABLE VII. Sequential triplet valence states for 2H-1,2,3-triazole; adiabatic and vertical excitation energies (eV), and second moments (a.u).[a,b]

| Energy (eV) | | Symmetry | State (decreasing density, $c_i^2$) | $\langle x^2\rangle$ | $\langle y^2\rangle$ | $\langle z^2\rangle$ |
|---|---|---|---|---|---|---|
| Adiabatic[c] | Vertical[c] | | $\tilde{X}^1A_1$ | −22.8 | −24.9 | −15.4 |
| 4.06 | 5.37 | $B_2$ | $1a_23b_1^* + 2b_12a_2^*$ | −22.9 | −24.4 | −17.1 |
| 4.98 | 5.48 | $A_1$ | $2b_13b_1^* - 1a_22a_2^*$ | −22.7 | −26.7 | −14.7 |
| 5.47 | 6.27 | $A_2$ | $6b_23b_1^* - 9a_12a_2^*$ | −24.0 | −21.8 | −16.9 |
| 6.01 | 6.69 | $B_2$ | $2b_12a_2^* - 1a_23b_1^*$ | −24.7 | −21.3 | −37.3 |
| 6.76 | 7.13 | $B_1$ | $9a_13b_1^* + 6b_22a_2^*$ | −24.1 | −22.9 | −16.1 |
| 7.49 | 7.87 | $A_1$ | $1a_22a_2^* + 2b_13b_1^*$ | −23.6 | −25.1 | −17.7 |
| 8.45 | 8.43 | $B_1$ | $6b_22a_2^* - 9a_13b_1^*$ | −24.6 | −22.6 | −17.4 |
| 8.67 | 9.15 | $A_2$ | $9a_12a_2^* + 6b_22a_2^*$ | −23.3 | −39.0 | −29.3 |

[a]B3LYP (−242.32319 a.u.) orbital occupancy $1a_1^2 - 9a_1^2 1b_2^2 - 6b_2^2\ 1b_1^2\ 2b_1^2 1a_2^2$.
[b]Singly occupied orbitals except where shown.
[c]Excitation energies are relative to the $\tilde{X}^1A_1$ ground state CASSCF energy −240.92831 a.u.
[d]Excitation energies are relative to the $\tilde{X}^1A_1$ ground state CI energy −241.59009 a.u.

suggested, following the readily observed *f*-Rydberg series for nitric oxide ($^2\Pi$ ground state, with singly occupied HOMO 2e). The explanation for the NO case,[4] is that under a united atom (UA) approach, the HOMO appears as an apparent $3d_\pi$-electron distribution at Rydberg orbital distances. The single-photon selection rule for orbital angular momentum of the excited electron, $\Delta l = \pm 1$, leads to an enhancement of the *np* and *nf* Rydberg series in the single-photon VUV absorption spectrum; this phenomenon is observed.[4,54] If we apply the UA approach here, then the $2b_1$ HOMO can be regarded as a $d_{XZ}$ MO on the *z*-axis at Rydberg distances, leading to an enhancement of *np* and *nf* Rydberg series. This is what we have observed with the *nd* series being very weak. It is interesting to note that the *nf* Rydberg series in furan is based on the $1a_2$ HOMO, which can certainly be regarded as having a $d_\pi$ character in the UA approximation.

## V. CONCLUSIONS

The VUV spectrum of **123T** shows a number of unusual features, both in terms of valence bands and Rydberg states. Analysis of the lowest UV band indicates the presence of one $\pi\pi^*$ and two $LP_N\pi^*$ bands; unexpectedly, much of the envelope of the 5.5 to 6.5 eV band shows fairly regular vibrational states despite the presence of three electronic states. This improbable finding suggests that a more complex phenomenon is occurring, leading to mixing of the three theoretical bands. The lowest singlet absorption shows that a nonplanar upper state occurs in the onset region, and the geometrical distortions to lower symmetry are important to the mixing of the states and the structure of this absorption band. The new determination of the UV photoelectron spectrum shows marked improvement in resolution for $IE_1$, and this improvement is critical for the determination of the $2b_1nf$ and other Rydberg states in the current VUV photoabsorption spectrum. Clearly *f*-orbitals must be included in any theoretical treatment. The present CI study, using a set of center-of-mass-based Rydberg functions, ensured that all *s, p, d, f* Rydberg states were treated equally in the study. With this computational methodology, we have achieved good agreement with the experiment for a number of low-lying Rydberg states.

The most variable bond upon excitation is the $C_4C_5$ bond. The 2H-1,2,3-triazole system can be thought of as a (NH) bridged buta-1,3-diene with diaza substitution (N replacing C), and this variability of the $C_4C_5$ bond is mirrored in the behavior of the central $C_2C_3$ bond in buta-1,3-diene.[18] The occurrence of nonplanarity in the upper state of the lowest absorption band mirrors that were found by Richardson *et al.*[29,30,38] and may have wider significance, such as to some other heterocyclic and aromatic compounds, where such issues have not been discussed.

## ACKNOWLEDGMENTS

We thank: (a) the UK National Grid Service (NGS) Operations Support Centre and the National Service for Computational Chemistry Software (NSCCS) for computing support; (b) Dr. P. Sherwood (Daresbury Laboratory) for maintenance of the GAMES-UK suite of programmes. D.L.L. thanks the National Science Foundation through the Project CHE-0749530. A.R.H. thanks the Department of Chemistry and Biochemistry, The University of Arizona, for support of the Molecular Photoelectron Spectroscopy facility. We thank a reviewer for helpful comments in relation to the *f*-Rydberg series being readily observed.

[1] F. Merkt, Annu. Rev. Phys. Chem. **48**, 675 (1997).
[2] G. Herzberg, *Molecular Spectra and Molecular Structure I: Spectra of Diatomic Molecules* (reprinted with corrections, Krieger Publishing Company, Malabar, Florida, 1991).
[3] G. Herzberg, *Molecular Spectra and Molecular Structure III: Electronic Spectra and Electronic Structure of Polyatomic Molecules* (Van Nostrand Reinhold, New York, 1966), pp. 415–419, 549–550, 656.
[4] E. Miescher and K. P. Huber, in *International Review of Science, Physical Chemistry*, edited by D. A. Ramsay, Series 2 (Butterworths, London, 1976), Vol. 3, pp 37–73.
[5] V. A. Shubert, M. Rednic, and S. T. Pratt, J. Chem. Phys. **132**, 124108 (2010).
[6] D. M. P. Holland, D. A. Shaw, M. Stener, and P. Decleva, J. Phys. B **42**, 245201 (2009).
[7] S. Yamamoto and H. Tatewaki, J. Chem. Phys. **132**, 054303 (2010).
[8] F. Laruelle, S. Boyé-Péronne, D. Gauyacq, and J. Liévin, J. Phys. Chem. A **113**, 13210 (2009).
[9] C. Escure, T. Leininger, and B. Lepetit, J. Chem. Phys. **130**, 244306 (2009).
[10] S. Eden, P. Limão-Vieira, S. V. Hoffmann, and N. J. Mason, Chem. Phys. **323**, 313 (2006).
[11] K. Siegbahn, C. Nordling, A. Fahlman, R. Nordberg, K. Hamrin, J. Hedman, G. Johansson, T. Bergmark, S. E. Karlsson, I. Lindgren, and B. Lindberg, Nova Acta Regiae Societatis Scientiarum Upsaliensis **20**, 282 (1967).
[12] M. A. Cranswick, A. Dawson, J. J. A. Cooney, N. E. Gruhn, D. L. Lichtenberger, and J. H. Enemark, Inorg. Chem. **46**, 10639 (2007).
[13] D. L. Lichtenberger, G. E. Kellogg, J. G. Kristofzski, D. Page, S. Turner, G. Klinger, and J. Lorenzen, Rev. Sci. Instrum. **57**, 2366 (1986).
[14] See supplementary material at http://dx.doi.org/10.1063/1.3549812 for additional expansions of the photoelectron and VUV photoabsorption spectra, more calculated structures, and expanded tables.
[15] M. F. Guest, I. J. Bush, H. J. J. Van Dam, P. Sherwood, J. M. H. Thomas, J. H. Van Lenthe, R. W. A. Havenith, and J. Kendrick, Mol. Phys. **103**, 719 (2005).
[16] P. J. Knowles, C. Hampel, and H. Werner, J. Chem. Phys. **99**, 5219 (1993).
[17] MOLPRO, a package of *ab initio* programs, version 2008.1, H.-J. Werner, P. J. Knowles, R. Lindh *et al.*
[18] M. H. Palmer and I. C. Walker, Chem. Phys. **373**, 159 (2010).
[19] R. J. Buenker and R. A. Phillips, J. Mol. Struct.: THEOCHEM **123**, 291 (1985).
[20] R. J. Buenker, in *Proceedings of the Workshop on Quantum Chemistry and Molecular Physics,Wollongong, Australia*, edited by P. G. Burton (University Press, Wollongong, 1980).
[21] R. J. Beunker, in *Current Aspects of Quantum Chemistry*, edited by R. Carbó (Elsevier, New York, 1982), Vol. 21, pp. 17–21.
[22] M. H. Palmer, G. Ganzenmüller, and I. C. Walker, Chem. Phys. **334**, 154 (2007).
[23] S. Cradock, R. H. Findlay, and M. H. Palmer, Tetrahedron **29**, 2173 (1973).
[24] G. L. Blackman, R. D. Brown, F. R. Burden, and W. Garland, J. Mol. Spectrosc. **65**, 313 (1977).
[25] M. Begtrup, C. J. Nielsen, L. Nygaard, S. Samdal, and C. E. Sjøgren, Acta Chem. Scand. **42A**, 500 (1988).
[26] M. H. Palmer, I. Simpson, and J. R. Wheeler, Z. Naturforsch., Pt. A **36a**, 1246 (1981).
[27] M. H. Palmer and A. J. Beveridge, Chem. Phys. **111**, 249 (1987).
[28] M. H. Palmer, Chem. Phys. **348**, 130 (2008).
[29] B. J. Forrest and A. W. Richardson, Can. J. Chem. **50**, 2088 (1972).
[30] E. Firkins and A. W. Richardson, J. Chem. Soc. D **21**, 1368 (1971).
[31] X. Amashukeli, N. E. Gruhn, D. L. Lichtenberger, J. R. Winkler, and H. B. Gray, J. Am. Chem. Soc. **126**, 15566 (2004).

[32]X. Amashukeli, J. R. Winkler, H. B. Gray, N. E. Gruhn, and D. L. Lichtenberger, J. Phys. Chem. A **106**, 7593 (2002).
[33]O. Lobanova Griffith, N. E. Gruhn, J. E. Anthony, B. Purushothaman, and D. L. Lichtenberger, J. Phys. Chem. C **112**, 20518 (2008).
[34]P. J. Derrick, L. Åsbrink, O. Edqvist, B. Jonsson, and E. Lindholm, Int. J. Mass Spectrom. Ion Phys. **6**, 191 (1971).
[35]P. J. Derrick, L. Åsbrink, O. Edqvist, and E. Lindholm, Spectrochim. Acta, Part A **27**, 2525 (1971).
[36]A. B. Trofimov, H. Koppel, and J. Schirmer, J. Chem. Phys. **109**, 1025 (1998).
[37]M. H. Palmer, Chem. Phys. **360**, 150 (2009).
[38]A. W. Richardson, Can. J. Chem. **52**, 100 (1974).
[39]M. B. Robin, *Higher Excited States of Polyatomic Molecules* (Academic, New York, 1974), Vol. 1.
[40]M. B. Robin, *Higher Excited States of Polyatomic Molecules* (Academic, New York, 1975), Vol. 2.
[41]M. B. Robin, *Higher Excited States of Polyatomic Molecules* (Academic, New York, 1985), Vol. 3.
[42]M. Bavia, F. Bertinelli, C. Taliani, and C. Zauli, Mol. Phys. **31**, 479 (1976).
[43]M. H. Palmer, I. C. Walker, and M. F. Guest, Chem. Phys. **238**, 179 (1998).
[44]M. H. Palmer, I. C. Walker, C. C. Ballard, and M. F. Guest, Chem. Phys. **192**, 111 (1995).
[45]T. Ridley, K. P. Lawley, M. H. S. N. Al-Kahali, and R. J. Donovan, Chem. Phys. Lett. **390**, 376 (2004).
[46]C. D. Cooper, A. D. Williamson, J. C. Miller, and R. N. Compton, J. Chem. Phys. **73**, 1527 (1980).
[47]M. H. Palmer and A. D. Nelson, Mol. Phys. **100**, 3601 (2002).
[48]M. Braunstein, R. L. Martin, and P. J. Hay, J. Chem. Phys. **102**, 3662 (1995).
[49]M. Braunstein and R. T. Pack, J. Chem. Phys. **96**, 6378 (1992).
[50]T. Ridley, K. P. Lawley, and R. J. Donovan, Phys. Chem. Chem. Phys. **6**, 5304 (2004).
[51]C. Chuang, C. Chen, H. Wu, and Y. Chen, Chem. Phys. Lett. **394**, 287 (2004).
[52]J. W. Raymonda, J. Chem. Phys. **56**, 3912 (1972).
[53]M. B. Robin, Chem. Phys. Lett. **119**, 33 (1985).
[54]Ch. Jungen and E. Miescher, Can. J. Phys. **47**, 1769 (1969); C. Jungen, J. Chem. Phys. **53**, 4168 (1970).